Low resistance at LiNi1/3Mn1/3Co1/302?and Li3P04?interfaces

著者	Kazunori Nishio, Naoto Nakamura, Koji Horiba, Miho Kitamura, Hiroshi Kumigashira, Ryota Shimizu, Taro Hitosugi
journal or publication title	Applied physics letters
volume	116
number	5
page range	053901
year	2020-02-03
URL	http://hdl.handle.net/10097/00131038

doi: 10.1063/1.5133879

Applied Physics Letters

Low resistance at $LiNi_{1/3}Mn_{1/3}Co_{1/3}O_2$ and Li_3PO_4 interfaces

Cite as: Appl. Phys. Lett. **116**, 053901 (2020); https://doi.org/10.1063/1.5133879
Submitted: 30 October 2019 . Accepted: 14 January 2020 . Published Online: 03 February 2020

Kazunori Nishio, Naoto Nakamura, Koji Horiba, Miho Kitamura, Hiroshi Kumigashira, Ryota Shimizu, and Taro Hitosugi

Applied Physics Letters ARTICLE scitation.org/journal/apl

Low resistance at $LiNi_{1/3}Mn_{1/3}Co_{1/3}O_2$ and Li_3PO_4 interfaces

Cite as: Appl. Phys. Lett. **116**, 053901 (2020); doi: 10.1063/1.5133879
Submitted: 30 October 2019 · Accepted: 14 January 2020 ·
Published Online: 3 February 2020

Kazunori Nishio,[1,a)] Naoto Nakamura,[1] Koji Horiba,[2] Miho Kitamura,[2] Hiroshi Kumigashira,[2,3] Ryota Shimizu,[1,4] and Taro Hitosugi[1]

AFFILIATIONS

[1]School of Materials and Chemical Technology, Tokyo Institute of Technology, Tokyo 152-8552, Japan
[2]Photon Factory, Institute of Materials Structure Science, High Energy Accelerator Research Organization (KEK), 1-1 Oho, Tsukuba, Ibaraki 305-0801, Japan
[3]Institute of Multidisciplinary Research for Advanced Materials, Tohoku University, Sendai 980-8577, Japan
[4]Department of Research Promotion, JST-PRESTO, Tokyo 102-0076, Japan

[a)]Author to whom correspondence must be addressed: nishio.k.ag@m.titech.ac.jp

ABSTRACT

We report the low resistance observed at the interface of $LiNi_{1/3}Mn_{1/3}Co_{1/3}O_2$ (NMC) and Li_3PO_4. First, we show the deposition of high-quality single-phase NMC (001) epitaxial thin films on Al_2O_3 (0001) substrates using pulsed laser deposition. Controlling the oxidation states of the three transition metals in NMC films is crucial for stable battery operation. However, in general, it is very difficult to simultaneously control the oxidation states of three elements in vacuum deposition processes. Tuning the oxygen partial pressure and temperature during deposition led to the growth of NMC thin films with ideal oxidation states (Ni^{2+}, Mn^{4+}, and Co^{3+}), as confirmed using bulk-sensitive x-ray excited optical luminescence. Next, using the NMC epitaxial thin films, we prepared solid-state batteries that demonstrated stable operation and very low resistance at the solid electrolyte/electrode interfaces. These results provide insight into the fabrication of multi-transition-metal electrode thin film materials, which are important for investigating the mechanisms of lithium battery operation. Furthermore, the low interface resistance indicates that Li_3PO_4 and oxide electrode materials form very stable low-resistance interfaces.

Although solid-state Li batteries have been attracting considerable attention, the electrochemical reaction at the electrolyte and electrode interfaces is still not well understood.[1] $LiNi_{1/3}Mn_{1/3}Co_{1/3}O_2$ (NMC) is known to exhibit excellent performance (high capacity, long cyclability, and high energy density) compared to $LiCoO_2$.[2] However, the resistance of the solid-electrolyte and NMC interface has not been fully studied. Investigations on interface resistance would lead to better strategies for optimizing the capabilities for fast charging and discharge of solid-state Li batteries.

For this purpose, epitaxial thin films of positive electrode materials play an important role, as they can serve as a model electrode for investigating interface phenomena between the electrodes and electrolytes.[3,4] Epitaxial thin films have well-defined surface areas, crystal orientations, and interface structures, opening a way to evaluate the interface resistance quantitatively via analysis of the electrochemical impedance spectrum.[5] Furthermore, the flat surfaces of epitaxial thin films enable chemical reactions to be studied using state-of-the-art characterization techniques.[6,7] Although synthesis of single-phase NMC epitaxial thin films has been reported,[8–10] few studies have addressed the crystallinity of thin films. The main difficulty in fabricating such films involves controlling the oxidation states of the three transition metals. To achieve stable battery operation, the oxidation states of the thin film NMC transition metals should be Ni^{2+}, Mn^{4+}, and Co^{3+}. Tuning the oxidation states is difficult during physical vapor deposition processes because the films are usually grown at oxygen partial pressures (P_{O2}) much lower than 10^5 Pa; it is quite difficult to tune the oxidation states independently. In addition, control of cation ordering is of crucial importance for achieving stable battery operation.

In this study, we report the low resistance at the interface of Li_3PO_4 and NMC epitaxial thin films. The (001)-oriented NMC epitaxial thin films were fabricated using pulsed laser deposition (PLD). We carefully controlled the oxidation states of the transition metals by tuning P_{O2} and the substrate temperature (T_s). We used bulk-sensitive

x-ray absorption spectroscopy (XAS) to probe the oxidation states of the transition metals inside the NMC epitaxial films. These measurements confirmed that the ideal oxidation states of Ni, Mn, and Co were achieved in the films. Finally, we demonstrate low solid-electrolyte/electrode interface resistances (10.2 Ω cm^2) and show the stable operation of solid-state batteries fabricated using the NMC epitaxial films.

Epitaxial thin films of NMC were synthesized using the PLD technique. A KrF excimer laser (wavelength: 248 nm, pulse duration: ~20 ns, repetition frequency: 5 Hz, spot size: 0.039 cm^2, and fluence: 0.7 J/cm^2) was used to ablate a polycrystalline target of $Li_{1.2}Ni_{1/3}Mn_{1/3}Co_{1/3}O_{2+\delta}$ (Toshima Manufacturing Co., Ltd.). The laser intensity at the target was monitored before growth.[11] The target–substrate distance was approximately 47 mm. NMC thin films were deposited on Al_2O_3 (0001) substrates (5 × 5 mm^2 and 0.5 mm thick) with a step and terrace surface obtained by annealing the substrate at 1000 °C for 3 h in air. The values of T_s and P_{O2} during NMC thin film growth were varied in the ranges of 500–700 °C and 10–100 mTorr, respectively.

Thin film quality was evaluated by x-ray diffraction (XRD) using a D8 Discover diffractometer (Bruker) equipped with a Ge (220) monochromator and a Cu target ($\lambda = 1.5406$ Å). Raman spectroscopy (532 nm excitation line; NRS-4100, Jasco) was used to identify the impurities in the thin films. The chemical compositions of the NMC thin films were determined by combining Rutherford backscattering spectroscopy (RBS) and particle-induced x-ray emission (PIXE). To investigate the oxidation states of the transition metal ions in the NMC thin films, XAS measurements were performed on a photoelectron spectrometer at beamline BL-2A MUSASHI of the Photon Factory, High Energy Accelerator Research Organization (KEK). To clarify the oxidation states of the NMC thin films, XAS spectra were obtained in transmission mode using x-ray excited optical luminescence from the Al_2O_3 substrates (bulk-sensitive mode). The samples were exposed to air during their transfer to the beamline. Ni L-edge, Mn L-edge, and Co L-edge spectra were scaled based on the reported values for the peaks with the maximum absorption intensities (~843, ~640, and 780 eV, respectively).[12]

We prepared thin-film batteries using the NMC epitaxial thin films. The NMC thin-film batteries were fabricated using an *in vacuo* process (the samples were never exposed to air),[13] providing a clean solid electrolyte/electrode interface. We used a $LaNiO_3$ epitaxial thin film, deposited using PLD, as the current collector. Detailed descriptions of the deposition of $LaNiO_3$ current collectors, Li_3PO_4 thin-film electrolytes, and Li negative electrodes can be found in our earlier report.[14] The thin-film battery performance was investigated using a potentio-galvanostat (VSP, Bio-Logic SAS) under a base pressure of 10^{-7} Torr.

We compared the growth of NMC epitaxial thin films for two different P_{O2} values: 10 and 100 mTorr. Figures 1(a) and 1(b) show the out-of-plane XRD patterns of the NMC films grown at $P_{O2} = 10$ mTorr (thickness: ~90 nm) and 100 mTorr (thickness: ~60 nm), respectively. At all T_s (500, 600, and 700 °C) and P_{O2} values studied, NMC thin films with (001) orientation were synthesized, as evidenced by the 00*l* diffractions attributed to the layered rock salt structure (space group $R\bar{3}m$) in the trigonal setting. Furthermore, in-plane XRD measurements confirmed the epitaxial growth of thin films (Fig. S1).

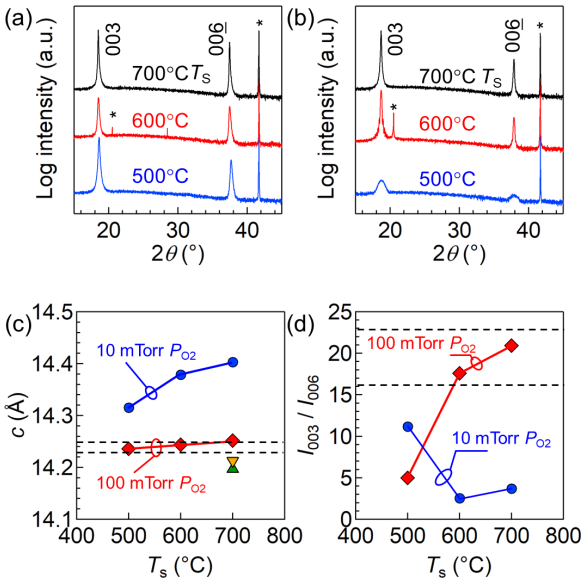

FIG. 1. Out-of-plane x-ray diffraction (XRD) patterns of $LiNi_{1/3}Mn_{1/3}Co_{1/3}O_2$ (NMC) thin films grown at various temperatures under partial oxygen pressures (P_{O2}) of (a) 10 mTorr and (b) 100 mTorr. (c) Substrate temperature (T_s) dependence of the *c*-axis lattice constant for NMC thin films grown at $P_{O2} = 10$ mTorr (blue circles) and 100 mTorr (red diamonds). The yellow triangle corresponds to the NMC thin film annealed at 500 °C for 5 h under $P_{O2} = 100$ mTorr after deposition of the film at $P_{O2} = 10$ mTorr. The green inverted triangle corresponds to the NMC thin film annealed at 480 °C for 5 h in air after deposition at $P_{O2} = 10$ mTorr. The horizontal dashed lines represent the typical reference bulk values for the *c*-axis lattice parameters. (d) Temperature dependence of the XRD intensity ratio of the 003 and 006 peaks (I_{003}/I_{006}) of NMC thin films. The dashed lines represent the reported bulk values for I_{003}/I_{006}.

The temperature dependence of the *c*-axis lattice constants of the films deposited at $P_{O2} = 10$ and 100 mTorr is presented in Fig. 1(c). For the NMC thin films grown at $P_{O2} = 10$ mTorr, the increase in T_s from 500 °C to 700 °C led to a monotonic increase in the *c*-axis lattice constant from 14.32 to 14.40 Å. These values were larger than the reference bulk *c*-axis lattice parameters [typically 14.227–14.247 Å, as indicated by dashed lines in Fig. 1(c)],[2,15–17] suggesting that oxygen vacancies were present in the films.[18] Oxygen vacancies are known to be unfavorable to battery operation.[2] It has been reported that annealing treatments are effective for enhancing the quality in $LiCoO_2$ epitaxial thin films by decreasing the amount of oxygen vacancies,[19] and accordingly, to reduce the amount of oxygen vacancies, we annealed the NMC thin films.

Two types of annealing treatments (500 °C in $P_{O2} = 100$ mTorr for 2 h and 480 °C in air for 5 h) were performed using identical samples grown at $P_{O2} = 10$ mTorr and $T_s = 700$ °C. After annealing, the *c*-axis lattice constants decreased to 14.20 Å (annealed at $P_{O2} = 100$ mTorr) and 14.21 Å (annealed in air). As the lattice parameters of the NMC thin films after annealing were similar to those of the bulk, we expect that the amount of oxygen vacancies decreased. However, Raman spectroscopy revealed that the annealed films had impurity phases, as discussed later.

Because oxygen vacancies were present in the as-grown films deposited at $P_{O2} = 10$ mTorr and because impurity phases were found

in the annealed films, we increased the P_{O2} to 100 mTorr. In contrast to the trend observed for the NMC films grown at $P_{O2} = 10$ mTorr, the *c*-axis lattice constants of the films grown at $P_{O2} = 100$ mTorr only exhibited a small T_s dependence. The *c*-axis lattice constants were in the range of 14.24–14.25 Å, in good agreement with the reference bulk values [Fig. 1(c)],[15–17] suggesting that the formation of oxygen vacancies was suppressed at $P_{O2} = 100$ mTorr.

The degree of cation ordering in the thin films was evaluated using the XRD intensity ratios of the 003 and 006 peaks (I_{003}/I_{006}). The α-$NaFeO_2$ structure $LiMO_2$ (*M* represents a transition metal such as Co, Ni, or Mn) has a highly ordered cation sublattice in which Li and *M* ions occupy alternating {111} layers of octahedral sites in a nearly cubic close-packed oxygen sublattice. The film quality degrades when *M* ions occupy Li sites and vice versa; such disordering of Li and *M* ions accompanies a transformation to a spinel or rock salt-like structure.[20,21] Accordingly, the I_{003}/I_{006} values are a measure of cation ordering, with a larger value indicating higher ordering.[22]

Figure 1(d) shows the I_{003}/I_{006} values for the synthesized NMC thin films. For the films deposited at $P_{O2} = 100$ mTorr, the I_{003}/I_{006} values increased as T_s increased, reaching 17.6 and 20.9 at 600 °C and 700 °C, respectively. These values agree well with the reported reference bulk values [dashed lines, Fig. 1(d)].[16,23,24] Thus, a higher T_s promoted ideal cation ordering along with sufficient oxidation.

Next, the film quality was investigated using Raman spectroscopy, which has a higher sensitivity to impurities than XRD. The Raman spectra indicated that the NMC thin films grown at $T_s = 700$ °C and $P_{O2} = 100$ mTorr were single phase. The spectrum showed the NMC A_{1g} peak at 602 cm^{-1} [Fig. 2(a)], matching well with earlier reports on bulk samples.[25] No impurities, such as Co_3O_4, were observed in the as-deposited films.

In contrast, we observed an impurity phase in the annealed films. The NMC thin film grown at $T_s = 700$ °C and $P_{O2} = 10$ mTorr exhibited a broad feature with a maximum peak intensity at ~581 cm^{-1}, which could be attributed to the A_{1g} mode of NMC with an expanded lattice. Annealing this sample at 500 °C in $P_{O2} = 100$ mTorr for 2 h induced the formation of Co_3O_4, as indicated by peaks in the Raman spectrum at 528 cm^{-1} and 695 cm^{-1} [Fig. 2(a)]. The Raman spectrum of the sample annealed in air at 480 °C for 5 h also showed an impurity phase [492 cm^{-1}, Fig. 2(a)] although the Co_3O_4 impurity phase disappeared. This impurity may be either $LiNi_{1-x}Co_xO_2$ ($x \leq 1$) or $LiNi_{1-y}Mn_yO_2$ ($y \leq 0.5$).[26,27]

The XRD patterns and Raman spectra indicate that a highly crystalline single-phase NMC thin film was obtained at $T_s = 600$ °C and $P_{O2} = 100$ mTorr. The XRD pattern of this film showed a fringe indicative of a flat surface [Fig. 2(b)], and the full width at half maximum of the 003 diffraction peak in the typical rocking curve was 0.089° (Fig. S1). The composition of transition metal ions, measured using RBS and PIXE, confirmed that this film was $LiNi_{1/3}Mn_{1/3}Co_{1/3}O_2$ (Fig. S2).

The oxidation states of the transition metals in the NMC thin film grown at $T_s = 600$ °C and $P_{O2} = 100$ mTorr (thickness: 60 nm) were investigated using bulk-sensitive XAS (Fig. 3). Each XAS spectrum exhibited two main peaks corresponding to the L_2 and L_3 edges, which originate due to the transitions of $2p_{1/2}$ and $2p_{3/2}$ core electrons to an unoccupied 3d level. Sharp spectra were observed for all the transition metals of Ni, Mn, and Co in the interior, indicating ideal Ni^{2+}, Mn^{4+}, and Co^{3+} states (Fig. 3). In contrast, when preparing an NMC thin film (thickness = 60 nm) grown under a reducing condition ($T_s = 700$ °C and $P_{O2} = 10$ mTorr), we confirmed the coexistence of Mn^{3+} and Co^{2+} in the NMC through XAS spectra (Fig. S3). Therefore, we fabricated NMC epitaxial thin films with ideal oxidation states.[12]

Finally, we fabricated thin-film batteries using the NMC epitaxial thin films. The batteries consisted of a $LaNiO_3$ current collector deposited on $SrTiO_3$(111), an NMC cathode, a Li_3PO_4 electrolyte, and a Li anode. The fabrication methods are summarized in the supplementary material (S4). Figure 4(a) shows charge and discharge curves over 20 cycles at the current density of 10 $\mu A\ cm^{-2}$. Except for the first charging, charge and discharge curves overlap, indicating the good cycle performance. However, the specific capacity after the 20th cycle showed approximately 150 mAh/g, which was less than the theoretical value (~200 mAh/g). Further research is required to identify the origin of the low capacity.

Figure 4(b) shows cyclic voltammograms of the battery over 20 cycles. Oxidative and reductive current peaks corresponding to the insertion/extraction of Li ions in NMC were observed. Although the first cycle showed a larger current at 3.81 V vs Li/Li^+, the cyclic voltammograms obtained between the second and twentieth cycles overlapped consistent with charge and discharge curves, indicating superior stability and repeatability during battery operation.

Figure 4(c) shows the impedance spectra at voltages of 2.5 V vs Li/Li^+ (discharging state) and 3.8 V vs Li/Li^+ (charging state). In both

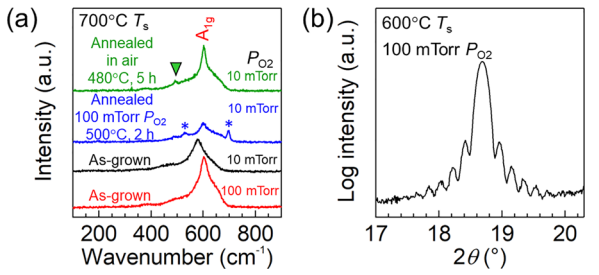

FIG. 2. (a) Raman spectra of $LiNi_{1/3}Co_{1/3}Mn_{1/3}O_2$ (NMC) thin films. (Black) The as-grown thin film fabricated at a substrate temperature (T_s) of 700 °C and an oxygen partial pressure (P_{O2}) of 10 mTorr. (Blue) The film after annealing at 500 °C and $P_{O2} = 100$ mTorr for 2 h. The blue asterisks indicate the peaks of an impurity [Co_3O_4; F_{2g} (528 cm^{-1}) and A_{1g} (695 cm^{-1})]. (Green) The film after annealing at 480 °C in air for 5 h. The inverted triangle indicates the impurity phase. (Red) The as-grown thin film fabricated at $T_s = 700$ °C and $P_{O2} = 100$ mTorr. (b) XRD pattern of the NMC thin film grown at $T_s = 600$ °C and $P_{O2} = 100$ mTorr.

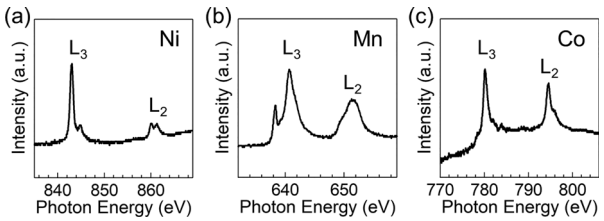

FIG. 3. X-ray absorption spectroscopy (XAS) spectra of a $LiNi_{1/3}Mn_{1/3}Co_{1/3}O_2$ (NMC) epitaxial thin film measured using the x-ray excited optical luminescence technique. (a) Ni L-edge, (b) Mn L-edge, and (c) Co L-edge. The NMC thin film was deposited at a substrate temperature of 600 °C and an oxygen partial pressure of 100 mTorr.

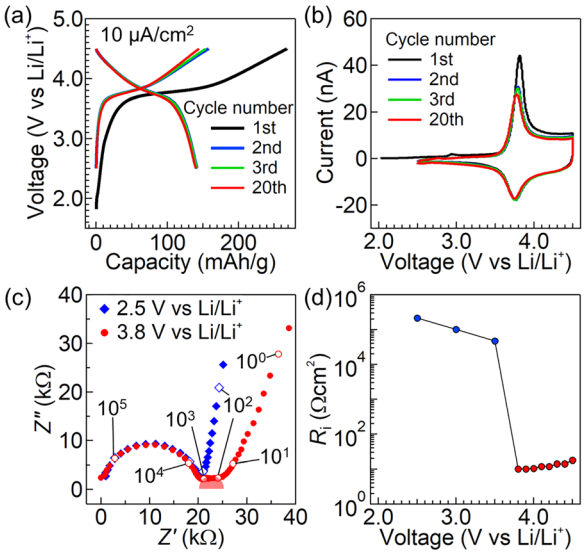

FIG. 4. Performance of the Li (1 μm)/Li_3PO_4 (250 nm)/$LiNi_{1/3}Mn_{1/3}Co_{1/3}O_2$ (40 nm)/$LaNiO_3$ (15.5 nm)/$SrTiO_3$ (111) thin-film battery. (a) Charge and discharge curves over 20 cycles (current density: 10 μA cm^{-2}). (b) Cyclic voltammograms over 20 cycles (scan rate: 1 mV/s). (c) Nyquist plots of impedance spectra in the discharging state (2.5 V vs Li/Li^+, blue diamonds) and the charging state (3.8 V vs Li/Li^+, red circles). The numbers indicate the corresponding frequencies (Hz). (d) Interface resistance values (R_i) at a variety of voltages.

the discharging and charging states, a clear semicircle was observed in the high-frequency region (1×10^3 to 3×10^5 Hz). This semicircle was assigned to the impedance of the Li_3PO_4 electrolyte because this semicircle was observed in both charged and discharged states and because the frequency range matched well with previous reports.[13,14] Moreover, the evaluated ionic conductivity of Li_3PO_4 was 6.4×10^{-7} S/cm, which agrees well with a previously reported value.[28]

In the charging state, another semicircle emerged in the frequency range of 10^2–10^3 Hz, shown as a red semicircle in Fig. 4(c). This second semicircle originated from the Li_3PO_4/NMC interface resistance, as the observed frequency range was consistent with our previous studies of $Li_3PO_{4-x}N_x$/$LiCoO_2$ and Li_3PO_4/$LiNi_{0.5}Mn_{1.5}O_4$ interfaces.[13,14] The evaluated resistance and the capacitance of the Li_3PO_4/NMC interface were 10.2 Ω·cm^2 and 2×10^{-7} F, respectively (simulation methods using an equivalent circuit model are described in the supplementary material). This extremely low interface resistance was comparable to those observed in our previous studies using $LiCoO_2$,[13,29] $LiNi_{0.5}Mn_{1.5}O_4$,[14] and $LiNi_{0.8}Co_{0.2}O_2$.[19] In addition, the value was very close to that reported for liquid-electrolyte/NMC interfaces (≥5 Ω·cm^2)[30] and much smaller than that reported for solid-electrolyte/NMC interfaces (>250 Ω·cm^2).[23,31]

Further, the interface resistances at a variety of voltages were evaluated. Figure 4(d) shows the interface resistance values at a variety of voltages. The resistances exhibited extremely large values greater than 47 kΩ cm^2 when the voltages were less than 3.6 V vs Li/Li^+ [blue circles in Fig. 4(d)]. In contrast, the values dramatically decreased ranging from 10.2 to 18.1 Ω cm^2 between 3.8 and 4.5 V vs Li/Li^+ [red circles in Fig. 4(d)]. At these voltages, electrochemical reactions occur with low interface resistances [Fig. 4(b)].

In conclusion, we synthesized high-quality NMC (001) epitaxial thin films on Al_2O_3 (0001) substrates using PLD. The transition metals in the thin films were in the ideal oxidation states of Ni^{2+}, Co^{3+}, and Mn^{4+}. Using the high-quality NMC thin films, the Li_3PO_4 and NMC film interfaces showed low-resistance values, similar to $LiCoO_2$, $LiNi_{0.5}Mn_{1.5}O_4$, and $LiNi_{0.8}Co_{0.2}O_2$. These results indicate that the formation of a low-resistance interface is universal for the combination of Li_3PO_4 solid-electrolyte and oxide electrode materials.

See the supplementary material for the XRD patterns and Raman spectrum of the best quality NMC thin film on Al_2O_3 (0001) (S1), RBS and PIXE analysis of the NMC thin film (S2), XAS spectra of NMC thin films (S3), fabrication methods for thin-film lithium batteries (S4), and evaluation of interface resistances and capacitances at a variety of voltages through impedance spectra analysis (S5).

This research was supported by JST-CREST Grant No. JPMJCR1523 and Toyota Motor Corporation. K.N. acknowledges funding from JSPS Kakenhi Grant Nos. 17H06674 and 18K14314. T.H. acknowledges funding from JKA Grant No. 109 and JSPS Kakenhi Grant No. 18H03876. We thank Toray Research Center, Inc. for the RBS-PIXE measurements. Raman spectroscopy measurements were performed at Ookayama Materials Analysis Division, Technical Department, Tokyo Institute of Technology. We would like to thank Editage (www.editage.jp) for English language editing.

REFERENCES

[1]M. Armand and J.-M. Tarascon, Nature **451**, 652–657 (2008).
[2]N. Yabuuchi and T. Ohzuku, J. Power Sources **119-121**, 171–174 (2003).
[3]M. Hirayama, N. Sonoyama, T. Abe, M. Minoura, M. Ito, D. Mori, A. Yamada, R. Kanno, T. Terashima, M. Takano, K. Tamura, and J. Mizuki, J. Power Sources **168**, 493–500 (2007).
[4]M. Hirayama, H. Ido, K. S. Kim, W. Cho, K. Tamura, J. Mizuki, and R. Kanno, J. Am. Chem. Soc. **132**, 15268–15276 (2010).
[5]M. Haruta, S. Shiraki, T. Suzuki, A. Kumatani, T. Ohsawa, Y. Takagi, R. Shimizu, and T. Hitosugi, Nano Lett. **15**, 1498–1502 (2015).
[6]D. Takamatsu, Y. Koyama, Y. Orikasa, S. Mori, T. Nakatsutsumi, T. Hirano, H. Tanida, H. Arai, Y. Uchimoto, and Z. Ogumi, Angew. Chem., Int. Ed **51**, 11597–11601 (2012).
[7]D. Takamatsu, T. Nakatsutsumi, S. Mori, Y. Orikasa, M. Mogi, H. Yamashige, K. Sato, T. Fujimoto, Y. Takanashi, H. Murayama, M. Oishi, H. Tanida, T. Uruga, Y. Uchimoto, and Z. Ogumi, J. Phys. Chem. Lett. **2**, 2511–2514 (2011).
[8]M. Abe, K. Suzuki, H. Minamishima, K. Kim, S. Taminato, M. Hirayama, and R. Kanno, J. Jpn. Soc. Powder Powder Metallurgy **62**, 531–537 (2015).
[9]M. Hirayama, M. Abe, S. Taminato, Y. Araki, K. Suzuki, and R. Kanno, RSC Adv. **6**, 78963 (2016).
[10]M. Abe, H. Iba, K. Suzuki, H. Minamitani, M. Hirayama, K. Tamura, J. Mizuki, T. Saito, and Y. Ikuhara, J. Power Sources **345**, 108–119 (2017).
[11]T. Ohnishi, H. Koinuma, and M. Lippmaa, Appl. Surf. Sci. **252**, 2466–2471 (2006).
[12]M. G. Kim, H. J. Shin, J.-H. Kim, S.-H. Park, and Y.-K. Sun, J. Electrochem. Soc. **152**, A1320–A1328 (2005).
[13]M. Haruta, S. Shiraki, T. Ohsawa, T. Suzuki, A. Kumatani, T. Takagi, R. Shimizu, and T. Hitosugi, Solid State Ionics **285**, 118–121 (2016).
[14]H. Kawasoko, S. Shiraki, T. Suzuki, R. Shimizu, and T. Hitosugi, ACS Appl. Mater. Interfaces **10**, 27498–27502 (2018).
[15]Y. W. Tsai, B. J. Hwang, G. Ceder, H. S. Sheu, D. G. Liu, and J. F. Lee, Chem. Mater. **17**, 3191–3199 (2005).

[16]K. M. Shaju, G. V. S. Rao, and B. V. Chowdari, Electrochim. Acta **48**, 145–151 (2002).
[17]L. Zhang, X. Wang, T. Muta, D. Li, H. Noguchi, M. Yoshio, R. Ma, K. Takada, and T. Sasaki, J. Power Sources **162**, 629–635 (2006).
[18]X. Li, Y. J. Wei, H. Ehrenberg, F. Du, C. Z. Wang, and G. Chen, Solid State Ionics **178**, 1969–1974 (2008).
[19]K. Nishio, T. Ohnishi, M. Osada, N. Ohta, K. Watanabe, and K. Takada, Solid State Ionics **285**, 91–95 (2016).
[20]R. J. Gummow, M. M. Thackeray, W. I. F. David, and S. Hull, Mater. Res. Bull **27**, 327–337 (1992).
[21]E. Rossen, J. N. Reimers, and J. R. Dahn, Solid State Ionics **62**, 53–60 (1993).
[22]K. Sakamoto, M. Hirayama, H. Konishi, N. Sonoyama, N. Dupré, D. Guyomard, K. Tamura, J. Mizuki, and R. Kanno, Phys. Chem. Chem. Phys **12**, 3815–3823 (2010).
[23]N. Machida, J. Kashiwagi, M. Naito, and T. Shigematsu, Solid State Ionics **225**, 354–358 (2012).
[24]S.-K. Hu, G.-H. Cheng, M.-Y. Cheng, B.-J. Hwang, and R. Santhanam, J. Power Sources **188**, 564–569 (2009).
[25]R. E. Ruther, A. F. Callender, H. Zhou, S. K. Martha, and J. Nanda, J. Electrochem. Soc. **162**, A98–A102 (2015).
[26]M. Inaba, Y. Todzuka, H. Yoshida, Y. Grincourt, A. Tasaka, Y. Tomida, and Z. Ogumi, Chem. Lett. **24**, 889–890 (1995).
[27]N. K. Karan, J. J. Saavedra-Arias, D. K. Pradhan, R. Melgarejo, A. Kumar, R. Thomas, and R. S. Katiyar, Electrochem. Solid-State Lett. **11**, A135–A139 (2008).
[28]N. Kuwata, N. Iwagami, Y. Tanji, Y. Matsuda, and J. Kawamura, J. Electrochem. Soc. **157**, A521–A527 (2010).
[29]S. Shiraki, T. Shirasawa, T. Suzuki, H. Kawasoko, R. Shimizu, and T. Hitosugi, ACS Appl. Matter. Interfaces **10**, 41732–41737 (2018).
[30]D. Li, Y. Kato, K. Kobayakawa, H. Noguchi, and Y. Sato, J. Power Sources **160**, 1342–1348 (2006).
[31]K. Okada, N. Machida, M. Naito, T. Shigematsu, S. Ito, S. Fujiki, M. Nakano, and Y. Aihara, Solid State Ionics **255**, 120–127 (2014).